

Ionizable Amino Lipid Interactions with POPC: Implications for Lipid Nanoparticle Function

Ramezanzpour, M.¹, Schmidt, M.L.², Bodnariuc, I.^{3,4}, Kulkarni, J.A.^{5,6}, Leung, S.S.W.², Cullis, P.R.⁵, Thewalt, J.L.^{2,3},
Tieleman, D.P.¹

¹ Centre for Molecular Simulation, Department of Biological Sciences, University of Calgary, Calgary, AB T2N 1N4, Canada

² Department of Physics, Simon Fraser University, Burnaby, BC V5A 1S6, Canada

³ Department of Molecular Biology and Biochemistry, Simon Fraser University, Burnaby, BC V5A 1S6, Canada

⁴ Department of Chemistry, University of Calgary, Calgary, AB T2N 1N4, Canada

⁵ Department of Biochemistry and Molecular Biology, University of British Columbia, Vancouver, BC V6T 1Z3, Canada

⁶ Department of Medical Genetics, University of British Columbia, Vancouver, BC V6T 1Z3, Canada

A. Methods

A.1. Experimental Methods

A.1.1. Materials and Sample Preparation

Lipids

1-palmitoyl-d₃₁-2-oleoyl-sn-glycero-3-phosphocholine (POPC-d₃₁) was purchased in powder from Avanti Polar Lipids Inc. (Alabaster, AL). The POPC-d₃₁ was dissolved in 80/20 benzene/methanol (v/v) and then the solvent was removed under vacuum to obtain a completely dry powder. The ionizable cationic lipid 2,2-dilinoleyl-4-(2-dimethylaminoethyl)-[1,3]-dioxolane (KC2) [1] was donated by AlCana Technologies Inc., (Vancouver BC). KC2 came in an oil form and was not lyophilized prior to use. All lipids were stored at -20°C.

Buffers

HEPES buffer was prepared by dissolving the salts in deuterium depleted water (reagents from Bioshop Canada Inc., (Burlington, ON) and Sigma-Aldrich Canada (Oakville, ON) respectively). The pH was adjusted to the desired value by adding NaOH (EM Science, affiliates of Merck KGaA (Darmstadt, Germany)).

Preparation of multilamellar vesicles for ^2H NMR and SAXS

Appropriate amounts of each lipid were weighed out and the lipids were co-dissolved in 1-2 mL 80/20 (v/v) benzene/methanol. The solvent was removed in two steps: first N_2 gas was used to evaporate the bulk of the solvent until only a thin lipid film was left, then any residual solvent was eliminated by lyophilizing the sample using a strong vacuum pump for several hours or overnight (until the sample weight was stable).

Samples contained approximately 50 – 60 mg total lipids and were hydrated in an excess of 10 mM HEPES buffer (~625-650 μL) at the desired pH. A series of five freeze (in liquid N_2) – thaw (room temperature) – vortex cycles were performed to ensure sample homogeneity. The sample was then transferred into the NMR tube and/or a quartz capillary tube (Charles Supper Company Inc. (Natick, MA)) for X-ray analysis. Samples in NMR tubes were stored at -20°C . Samples for X-ray analysis were put into the capillary tube either immediately before the experiment or left in the fridge overnight, since the quartz capillary tubes were sealed with wax.

After the experiments under basic pH conditions were completed, the pH of the sample was changed inside the sample tube by adding an appropriate amount of glacial acetic acid (Anachemia Science Canada Inc. (Vancouver, BC)) and vortexing. The final pH was verified using pH paper.

Preparation of LNPs containing KC2 for Cryogenic Transmission Electron Microscopy

LNPs were prepared using a rapid mixing technique previously described [2]. Briefly, lipid components (POPC, Cholesterol and KC2) dissolved in ethanol were mixed at the appropriate ratios to a final lipid concentration of 20 mM. The lipids in ethanol were mixed with 25 mM sodium acetate buffer (pH 4) using a T-junction mixer [3-5]. The resulting suspension was dialysed against 1000-fold volumes of pH 4 buffer or phosphate buffered saline (PBS) overnight. The LNPs were then concentrated using 10kDa NWCO Amicon centrifugal filter units to a final lipid concentration of ~20 mg/mL and imaged by Cryo-TEM.

POPC liposomes produced using this technique are extremely small and poorly resolved by cryo-TEM. Additionally, it was shown that replacement of PC-lipid with ICLs resulted in decreased particle sizes [2]. Systems containing cholesterol are larger and thus can be imaged easily [6, 7]. Moreover, LNPs used in

drug delivery studies contain cholesterol. Thus, in order to study the effect of KC2(H) on nanoparticles (at sizes that are readily resolved by cryo-TEM) cholesterol was included in the formulation.

A.1.2. Deuterium NMR (^2H NMR)

^2H NMR experiments were performed using an Oxford 300 MHz magnet with a ^2H frequency of 46.8 MHz and a TecMag Scout (TecMag, Inc. (Houston, TX)) spectrometer. The standard quadrupolar echo pulse sequence was used. The two out of phase 90° pulses were $3.95 \mu\text{s}$ long, the interpulse delay was $40 \mu\text{s}$ and the recycle delay was 300 ms. Data was collected using 8-cycle CYCLOPS phase cycling. All temperatures investigated were well above the gel-fluid transition of POPC, and an equilibration time of 45 minutes was used for each 5 degree temperature increment. 50 000 scans were collected to ensure an adequate signal-to-noise ratio in the spectra that were de-Paked using the iterative method described by Sternin et al. [8].

The orientational order parameter of a C-D bond in the hydrocarbon chain, S_{CD} , is

$$|S_{CD}| = \left| \frac{\langle 3\cos^2\theta - 1 \rangle}{2} \right|$$

Equation 1

where θ is the angle between the C-D bond vector and the bilayer normal, and can be obtained from the spectrum via the relationship

$$\Delta\nu_Q = \frac{3}{4}(167\text{kHz})|S_{CD}|$$

Equation 2

where $\Delta\nu_Q$ is the quadrupolar splitting and 167 kHz is the quadrupolar coupling constant. The smoothed order parameter profiles were obtained experimentally by measuring the quadrupolar splittings of the de-Paked ^2H spectra [9].

A.1.3. Small Angle X-ray Scattering

Small angle X-ray scattering (SAXS) curves were obtained using a SAXSLAB Ganesha 300XL (Skovlunde, Denmark) setup with a Linkam variable temperature sample stage. The X-ray source was $\text{Cu-K}\alpha$ ($\lambda = 1.54 \text{ \AA}$). The Linkam stage sample-to-detector distance was calibrated using silver behenate and the temperature was calibrated using the pre-transition and chain melting transition temperatures of both DPPC and DMPC bilayers. Disposable thin-walled quartz capillary tubes (80 mm long, 1.5 mm (outer diameter), 0.01 mm thickness) were used to hold the samples. To ensure that the sample was equilibrated, two sets of data were typically collected at each temperature: one at 30 minutes and one at 60 minutes after the setpoint temperature was reached. Each data collection run was 600 s. Initial and final data were collected at the same temperature to check for any changes in the sample over the course of the temperature run.

The bilayer repeat spacing (d-spacing) was measured from the SAXS scattering curves using the following relationship

$$d = \frac{2\pi n}{q_{peak}} \quad \text{Equation 3}$$

where q_{peak} is the position of the peak and n is its order number. The peak order number depends on the symmetry of the system and in the case of stacked bilayers, $n = 1, 2, 3, 4, \dots$ [10].

A.1.4. Cryogenic Transmission Electron Microscopy (Cryo-TEM) of LNPs

Cryo-TEM was performed as previously described [2]. Briefly, 3-5 μL of concentrated LNP suspensions were added to glow-discharged copper grids. A FEI Mark IV Vitrobot (FEI, Hillsboro, OR) was used to plunge-freeze blotted grids into liquid ethane. Vitrified samples were stored under liquid nitrogen. Frozen grids were imaged using a FEI Tecnai G2 (FEI, Hillsboro, OR) operating at 200 kV in low-dose mode and images were obtained using an FEI Eagle 4K CCD camera (FEI, Hillsboro, OR). All sample preparation and imaging were performed at the University of British Columbia BioImaging Facility (Vancouver, BC).

A.2. Computational Methods

A.2.1. System construction

All systems were constructed using an in-house developed script based on GROMACS modules [11] as follows. For the binary mixtures, two monolayers each composed of only one lipid type were built first. Each monolayer was composed of 100 lipids distributed on a two-dimensional grid (10 by 10). Two GROMACS modules, *gmx editconf* and *gmx genconf*, were used to translate and rotate the lipids on each grid point. Next, a set of random numbers from 1 to 100 was generated to satisfy the desired mixing ratio. For instance, for POPC/KC2H (80/20), 20 random numbers were generated. These 20 numbers were used to both keep the KC2H in 20 grid points, and to delete the POPC in the same grid points. Finally, the coordinate files from two modified monolayers were merged resulting in one mixed monolayer with a desired mixing ratio; which was taken as the upper leaflet. Assuming this monolayer is in the XY-plane, its rotation (using *gmx editconf* module) around either the X or Y axis gives the lower leaflet. Adjusting the center of both leaflets to (0,0,0) and subsequently merging the coordinate files for these two leaflets resulted in the POPC/KC2H (80/20) bilayer. Waters were subsequently added on the top and bottom of this system. Finally, counter ions (Cl^-) were added to neutralize the systems composed of POPC and KC2H. For the neutral POPC/KC2 systems no ions were added. When excess ion concentration was of interest, structures at 200 ns from pure POPC simulations and 500 ns from POPC/KC2H simulations were extracted, and Na^+ and Cl^- ions were added to these structures to reach the 150 mM salt concentration.

The ternary mixtures of POPC/KC2(H)/cholesterol (25/30/45) were constructed using a similar approach. Three monolayers composed of 100 lipids of each of the three types were built and two sets of random numbers were generated, which were used to remove or keep the lipids from each type at each grid point.

A.2.2. Molecular dynamics simulations

All simulations were conducted using the GROMACS package (v. 2016.3) (see **Table S1** for a full list of systems simulated in this study). The CHARMM36 force field [12] was used to model the molecules in the system, and about 70 TIP3P water molecules [13, 14] were added to each system to fully hydrate the bilayer. Periodic boundary conditions were applied in all directions. A time step of 2 fs was used, and the coordinates were saved every 50000 steps. A semi-isotropic pressure coupling was applied to the system, with Z direction (the normal direction to the bilayer surface) treated independently from the XY- plane.

The Parrinello-Rahman pressure coupling [15, 16] with a time constant of 5.0 ps was used to keep the pressure at 1 bar. The temperature was maintained at either 288 K or 313 K using Nose-Hoover extended ensemble [17, 18]. The temperature for two groups of lipids and water plus ions were coupled separately using a time constant of 1 ps, and the center of mass translation of these groups were removed every 100 steps independently.

The nonbonded interactions were treated using the Verlet cutoff scheme. The van der Waals and Coulomb interactions were switched at 0.8 nm and 0.0 nm, respectively, with a cutoff at 1.2 nm. No dispersion correction was applied, and PME [19, 20] was used to treat the long-range electrostatic interactions after the cutoff. The force-switch and potential-shift functions were used as van der Waals and the Coulomb modifier functions, respectively. All bonds involving hydrogen atoms were constrained using the LINCS algorithm [21].

The other simulation parameters were mainly the ones recommended by CHARMM-GUI [22] for using C36 FF in GROMACS package for simulation of lipid bilayers, except that the van der Waals interactions were switched at 0.8 instead of 1.0 nm [23].

Pure POPC bilayer were simulated for 200 ns, whereas binary and ternary mixtures were simulated for 700 ns. The systems with 150 mM salt concentration were simulated for 300 ns [Table S1].

Table S1. Summary of simulations.

System	Mixing ratio	NaCl concentration (mM)	Simulation time (ns)
POPC	-----	0	200
POPC	-----	150	300
POPC/KC2	90/10 80/20 70/30	0	700
POPC/KC2H	90/10 80/20 70/30	0	700
POPC/KC2H	90/10 80/20 70/30	150	300

POPC/KC2/cholesterol	25/30/45	0	700
POPC/KC2H/cholesterol	25/30/45	0	700

A.2.3. Simulation Analysis

All analyses were performed using GROMACS (v. 2016.2) modules, except otherwise mentioned. The last 100 ns of each simulation was used for the analysis. VMD [24] and Xmgrace were used for generating the figures and graphs, respectively.

Deuterium order parameters: The S_{CD} parameters from all-atom simulations can be calculated according to **Equation 2**. In this case, the θ is the angle between the C-H bond in each methylene group in the POPC palmitoyl chain and the Z axis (the normal direction to the membrane surface), and the angular brackets represent the ensemble average. The script to calculate the S_{CD} from simulations was provided by Dr. Thomas Piggot [25].

Electron and number densities: All the electron/number densities were calculated using the *gmx density* module of the GROMACS package. The box in the Z direction (normal to the bilayer surface) was divided into 100 slices and the density was symmetrized along the Z axis.

POPC P→N vector angle distribution: The distribution of the angle between the POPC P→N vector and the vector normal to each bilayer leaflet pointing in the direction of the water phase was calculated using the *gmx gangle* module of the GROMACS package. The bin width was 0.5 degrees, and graphs show a

running average over 20 data points (10 degrees) to highlight the observed trend in tilt angle change due to KC2H concentration.

B. KC2 and KC2H parameterization in the CHARMM36 force field

Although the parameters for POPC are available, optimized and well-tested in C36 FF [12], the parameters for KC2 and KC2H are not present and need to be developed. The step-by-step protocol for parameterization of a novel molecule in C36 FF is documented in detail in several publications [26, 27]. In this study, several computational tools, including CHARMM-GUI [28], GAAMP [29], and ParamChem [30, 31] were used to develop reasonable models for KC2 and KC2H compatible with C36 FF.

The KC2(H) molecules were first divided into two main segments: lipid tails and headgroup. The parameters for the tails were simply taken from DUPC downloaded from CHARMM-GUI [28], with atom types taken from C36 FF. The headgroup was divided into two smaller segments (the ring and the amino segments) and each segment was parameterized using GAAMP server [29], with atom types taken from CHARMM General Force Field (CGenFF) [27]. The parameters developed for the segments were subsequently combined to give the parameter set for the whole lipid molecules [32]. Where needed, parameters were further modified iteratively until the desired level of agreement between computational and experimental data was achieved (see below).

B.1. KC2 and KC2H model validation

The amount of target data to validate parameters against is limited for the case of KC2 and KC2H. In this study, the effect of adding KC2(H) on POPC palmitoyl chain order parameters in POPC/KC2(H) mixtures at 313 K was used for KC2(H) model validation.

The S_{CD} profiles for the POPC palmitoyl chain extracted from 2H NMR spectra and calculated from simulations of POPC/KC2(H) binary mixtures are shown in **Figure S1**. In simulations, systems with KC2 and KC2H correspond to the 2H NMR experiments conducted at pH 8.1 and 4.4, respectively. The S_{CD} parameters from simulations are in good agreement with the experimental data. The overall trend in S_{CD}

profiles is similar between simulations and experiments. The acyl chain order gradually decreases along the acyl chain towards the terminal methyl group. Computational S_{CD} parameters are slightly higher than the corresponding experimental values. This is also true for POPC, with optimized and well tested parameters in C36 FF.

In both simulations and experiments, the pH seems to have no or little effect on acyl chain order parameter at 313 K. The only difference was observed between pure POPC bilayers at two pH values. We note that the experimental POPC palmitoyl chain order parameters are smaller at pH 4.4 than at pH 8.1. This is likely due to the higher interfacial surface tension observed in POPC membranes at pH 4.4 [33]. In simulations, however, the S_{CD} parameters for palmitoyl chain are the same between two pH levels. That is mainly because the effect of buffer and the higher surface tension were not considered in our simulations.

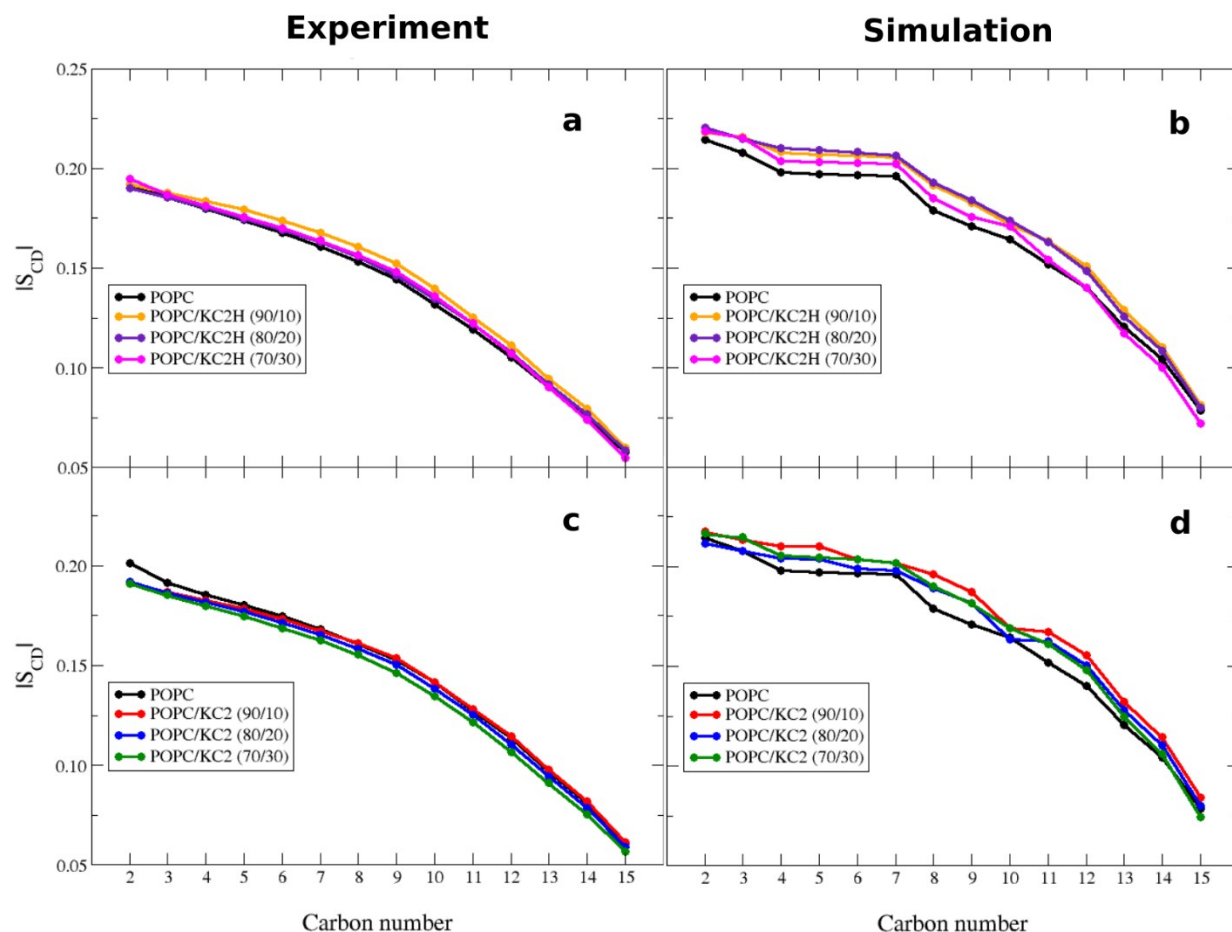


Figure S1. Validation of developed models for KC2 and KC2H. Smoothed deuterium order parameter (S_{CD}) profiles for the palmitoyl chain of POPC in POPC/KC2(H) binary mixtures were measured using ^2H NMR (**Left column**). The same parameter was calculated from simulations and smoothed (**Right column**). This comparison was done for two pH levels of 4.4 (**a** and **b**) and 8.1 (**c** and **d**) at temperature of 313 K.

C. KC2(H) effects on POPC acyl chains as a function of temperature and mixing ratio

The POPC- d_{31} order parameter (S_{CD}) profiles for POPC/KC2(H) systems at different temperatures and mixing ratios were measured using ^2H NMR. The effect of KC2 and KC2H on POPC *sn-1* acyl chain S_{CD} was shown to be a function of both temperature and mixing ratio [**Figure S2 and S3**]. For both pH 4.4 and 8.1, and all the mixing ratios studied, higher temperatures resulted in lower S_{CD} values as expected. For the pure POPC system, the POPC palmitoyl chain order parameters are significantly smaller at pH 4.4 than pH

8.1. At higher temperatures (303 K and 313 K), pH has little to no effect on chain order in POPC/KC2(H) systems. At 288 K and 293 K, KC2H has no effect on POPC chain order, while KC2 increases it.

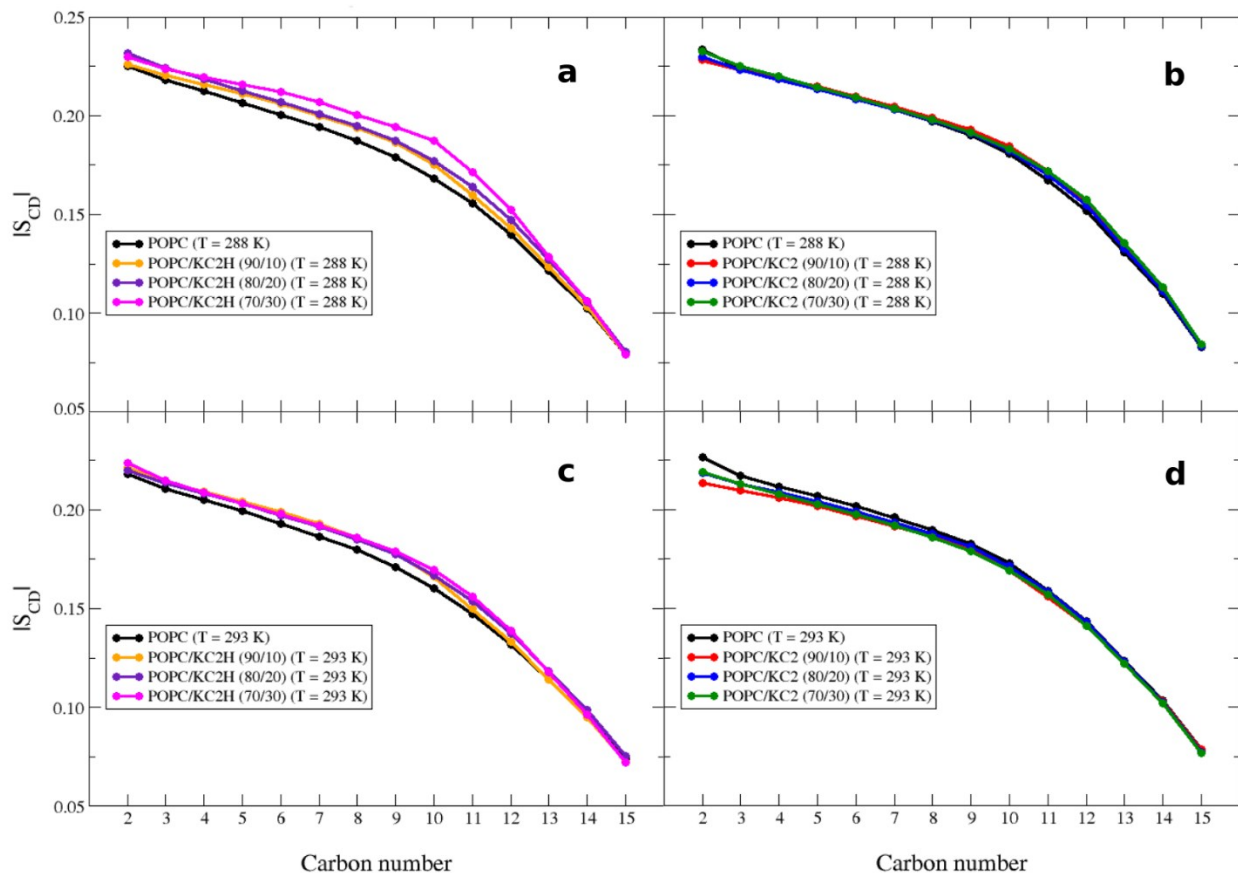


Figure S2. Deuterium order parameter (S_{CD}) profiles for the palmitoyl chain (*sn-1*) of POPC at 288 K and 293 K. Experimental ^2H NMR S_{CD} parameters (smoothed) for binary POPC/KC2(H) mixtures at (a) pH = 4.4 and T = 288 K, (b) pH = 8.1 and T = 288 K, (c) pH = 4.4 and T = 293 K, and (d) pH = 8.1 and T = 293 K.

Induced order in PC lipids due to the addition of cationic lipids has been previously reported [34]. The inclusion of cationic lipids (DMTAP) in a zwitterionic (DMPC) membrane was reported to induce acyl chain order in DMPC in a concentration-dependent way, up to 0.50 mole fraction of DMTAP [34]. Increasing the DMTAP mole fraction above 0.50, however, decreased the induced order. To explain this observation, the authors proposed a scenario as follows. Given that both DMTAP and DMPC have the same

acyl chains, a small amount of DMTAP tends to reorient the nearby DMPC headgroups tilt angle to smaller angles. This will result in more packed structures with a reduced area per lipid and increased acyl chain order. Upon increase in the DMTAP concentration beyond a limit, the electrostatic repulsions between the positively charged lipids dominate which result in the membrane surface expansion and a decrease in the acyl chain order.

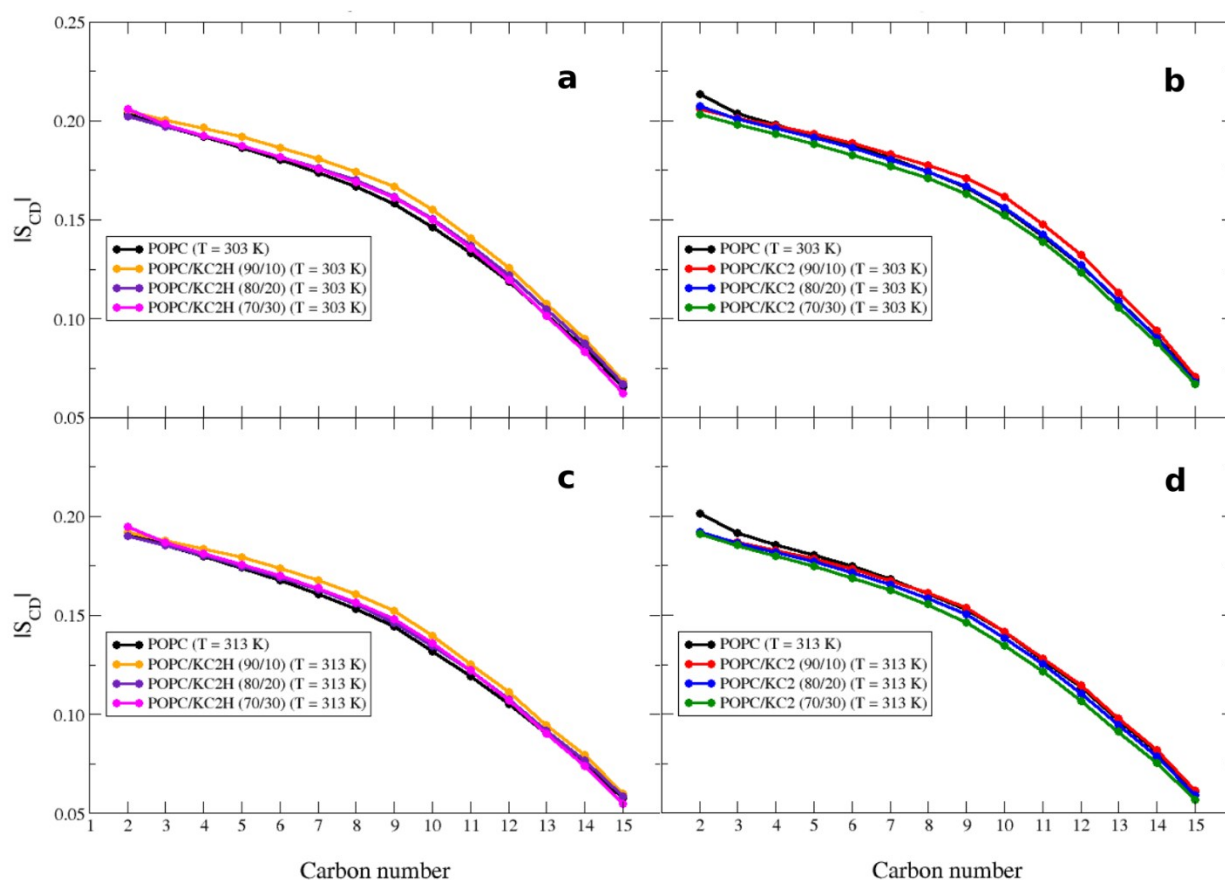


Figure S3. Deuterium order parameter (S_{CD}) profiles for the palmitoyl chain (*sn-1*) of POPC at 303 K and 313 K. Experimental ^2H NMR S_{CD} parameters (smoothed) for binary POPC/KC2(H) mixtures at (a) pH = 4.4 and T = 303 K, (b) pH = 8.1 and T = 303 K, (c) pH = 4.4 and T = 313 K, and (d) pH = 8.1 and T = 313 K.

The same scenario might also be valid here and could explain the induced chain order at pH 4.4 [Figure S2]. However, since the acyl chains in KC2H and POPC are not the same, the behavior of POPC/KC2H

systems is more complex to explain. This complicated pattern (i.e. temperature-concentration dependency) of induced order might be a collective effect of several factors, including the interfacial surface tension [33], which is likely relaxed due to KC2H, the observed decrease in POPC P→N vector tilt angle (see **section G**) [34], lipid-ion interactions (see **section F**) [35], and lipid-lipid interactions [34, 36]. Other factors might also contribute to such a complex behavior. The so-called free volume in the center of the bilayer [37] could be one such factor. In a study by Kupianien et al. [38], it was shown that a reduction in the free volume of membrane result in a tighter molecular packing and enhanced ordering of the acyl chains.

D. KC2(H) effect on POPC lamellar repeat spacing

If neutral KC2 are segregated and confined in the POPC bilayer center, systems with a higher concentration of KC2 are expected to result in systems with larger repeat spacings (*d*-spacing) at higher pH values. According to this expectation and the observations from simulations, SAXS experiments were carried out on POPC multilamellar vesicles containing 0, 20 or 30 mol% KC2 at pH 8.1, 8.5 and 10 [**Figure S4**]. The major finding is that the added KC2 causes a dramatic reduction in structure correlations in the sample, as exemplified by the broad scattering peak [**Figure S7**]. A second result is that the bilayer repeat spacing increases from 65 Å to 68 Å upon the addition of 20 mol % KC2 to POPC at pH 8.1. Increasing the pH to 8.5 results in a reduction in lamellar repeat spacing to 67.5 Å, and increasing the pH to 10 brings the lamellar repeat spacing back to 65 Å. These changes in lamellar repeat spacing can be explained by the presence of a small fraction of positively charged KC2H at pH 8.1 and 8.5, and are consistent with the observations of B. Pozo Navas et al. [39] on POPC/POPG mixtures. In our case, it is likely that the broad peaks are caused by KC2 separating into oily droplets associated with and disrupting the stacking regularity of the POPC lamellae.

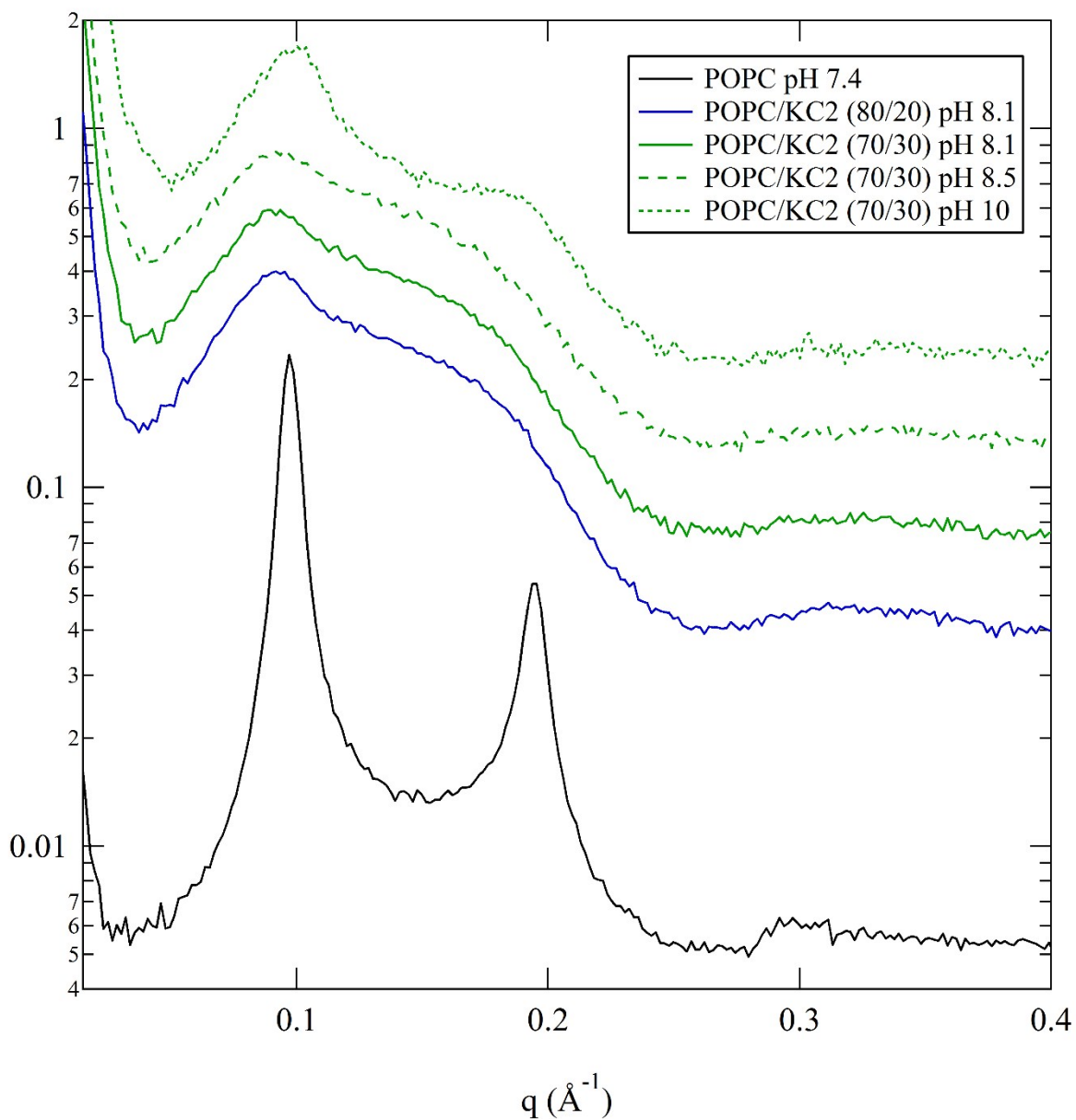


Figure S4. SAXS curves for POPC/KC2 multilamellar vesicles at several basic pH values. SAXS curves for POPC multilamellar vesicles containing 0, 20 or 30 mol % KC2 at the indicated pH levels. All scans were taken at 295.5 K.

E. KC2H stays in the lipid-water interface and has little to no effect on the POPC bilayer thickness

Regardless of the KC2H content in the mixtures, simulations suggest that all KC2H stay in the lipid-water interface [Figure 1]. Figure S5 shows the symmetrized electron densities for the POPC phosphorus atoms

in POPC/KC2H systems at different mixing ratios, pH = 4.4 and T = 313 K. For the pure POPC, the inter-leaflet distance is approximately 3.72 nm. Adding KC2H had little to no effect on POPC P-P distance.

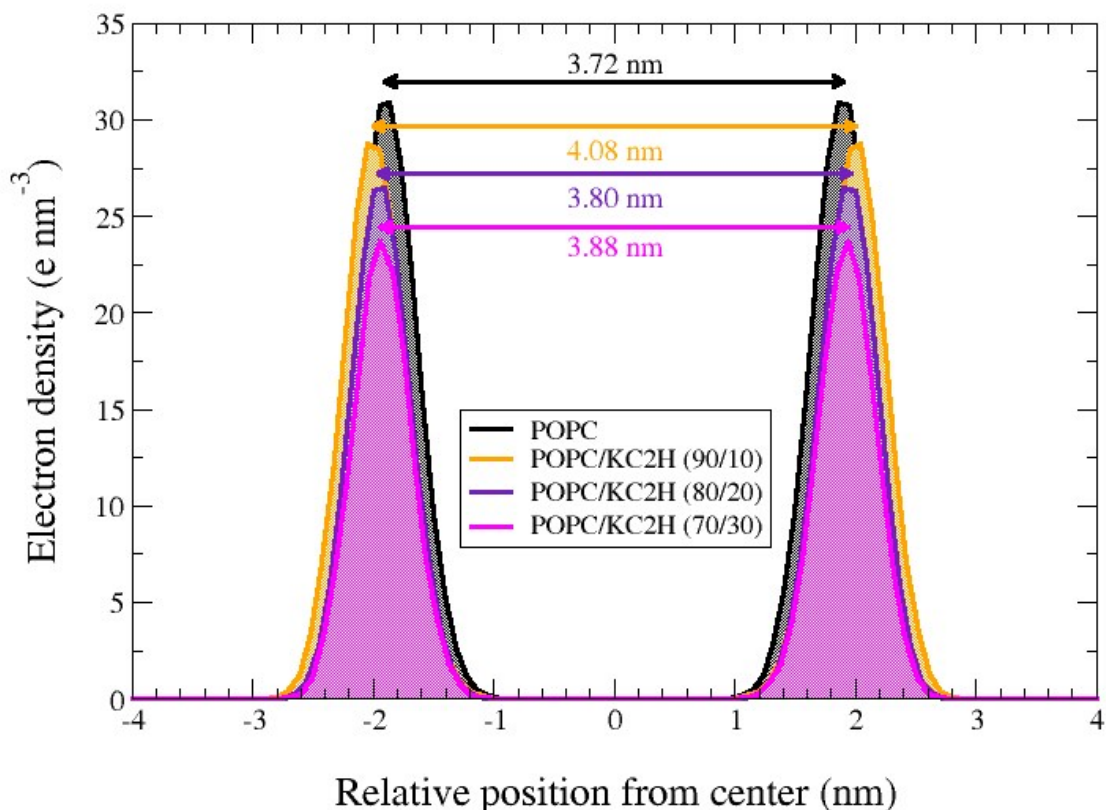


Figure S5. Effect of adding KC2H on POPC inter-leaflet distance. The electron density of the phosphorus atoms of POPC were calculated from simulations of binary POPC/KC2H mixtures at pH = 4.4 and T = 313 K. The X axis shows the relative distance from the bilayer center. Each double-headed arrow represents the peak-to-peak distance for a mixing ratio, corresponding to the P-P inter-leaflet distance. The P-P distance for the pure POPC system at 313 K is about 3.72 nm.

F. KC2H repels Na⁺ ions from and attracts Cl⁻ ions to the lipid-water interface

Given the positive charge of amino group in KC2H, electrostatic interactions with both negatively and positively charged groups (e.g. ions and POPC headgroups) in the system are expected. To study how

KC2H affect the structural properties of the system, we further investigated the ion distribution and POPC headgroup tilt angle as a function of KC2H concentration in the system at 313 K.

Electron densities for the Cl^- and Na^+ ions in POPC/KC2H systems simulated at acidic pH and temperature 313 K are shown in **Figure S6**. Adding KC2H to the system redistributes the ions. For the pure POPC system, the Cl^- ions density is zero from 0 to ca. 1.8 nm from the bilayer center [**Figure S6-a**]. It then increases smoothly and reaches its maximum at ca. 2.9 nm. Finally, it decreases slightly and reaches a plateau corresponding to a uniform distribution of ions in the aqueous phase. Adding KC2H to the POPC system populates the hydration layer with Cl^- ions. The Cl^- ion density in the hydration layer was directly correlated with the KC2H concentration in the bilayer. Furthermore, in the presence of KC2H, the peak corresponding to the maximum Cl^- ion density was shifted towards the bilayer center, compared to the pure POPC system.

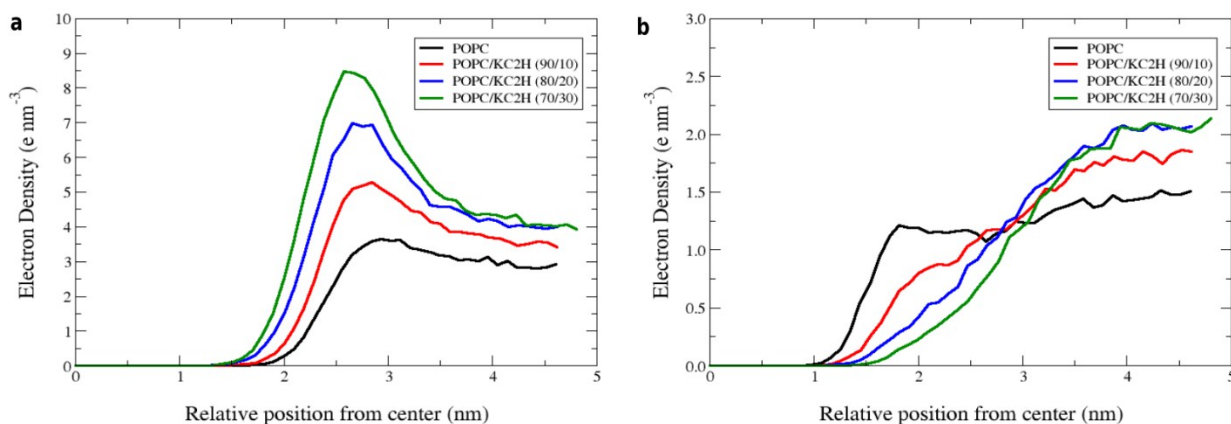


Figure S6. Effect of KC2H on ion distribution. Symmetrized electron densities of **a)** Cl^- and **b)** Na^+ ions for systems with different mixing ratios simulated at $\text{pH} = 4.4$ and $T = 313$ K. Assuming the bilayers are centered at zero, only the densities for the positive positions are shown. The X axis shows the direction normal to the bilayer surface.

Na^+ ions [**Figure S6-b**] are distributed deeper in the hydration layer, compared to the Cl^- ions. The Na^+ density peaks around 1.8 nm. The Na^+ density near the bilayer surface is slightly less than Na^+ density in aqueous phase. Adding KC2H to POPC repels the Na^+ ions from the bilayer.

The Cl⁻ and Na⁺ ions electron densities in pure POPC system [**Figure S6**] agree with previous studies on ion distributions in lipid bilayers [40, 41]. Na⁺ ions were found to be deeper in the hydration layer compared to Cl⁻ ions, as expected. **Figure S6** suggests that adding KC2H affects the ion distribution along the bilayer normal. Upon adding KC2H to the system, the Cl⁻ ions are attracted towards the lipid-water interface, while the Na⁺ ions are repelled from the interface. This behavior is also consistent with previous reports on membranes containing cationic lipids [34, 40]. Presence of positively charged KC2H in the membrane increases the effective positive charge of the membrane surface. This consequently attracts the negatively charged Cl⁻ ions and deplete the lipid-water interface from positively charged Na⁺ ions.

G. KC2H affects the POPC headgroup distribution

The tilt angle for the POPC headgroup (i.e. the angle between the POPC P→N vector and outward normal to the leaflet) were calculated for each system at 313 K and are shown in **Figure S7**. For the pure POPC simulations, this angle is approximately 70 degrees [**Figure S7**], in a close agreement with previous studies [23, 42, 43]. Adding KC2H to the POPC bilayers is shown to affect the distribution of POPC headgroups. More KC2H in the system resulted in smaller tilt angles so that the POPC choline group moves towards the aqueous phase. For instance, 30 mol% KC2H reduced this angle from ~ 70 to ~ 43 degrees. KC2, on the other hand, did not have any effect on the average POPC headgroup angle distribution.

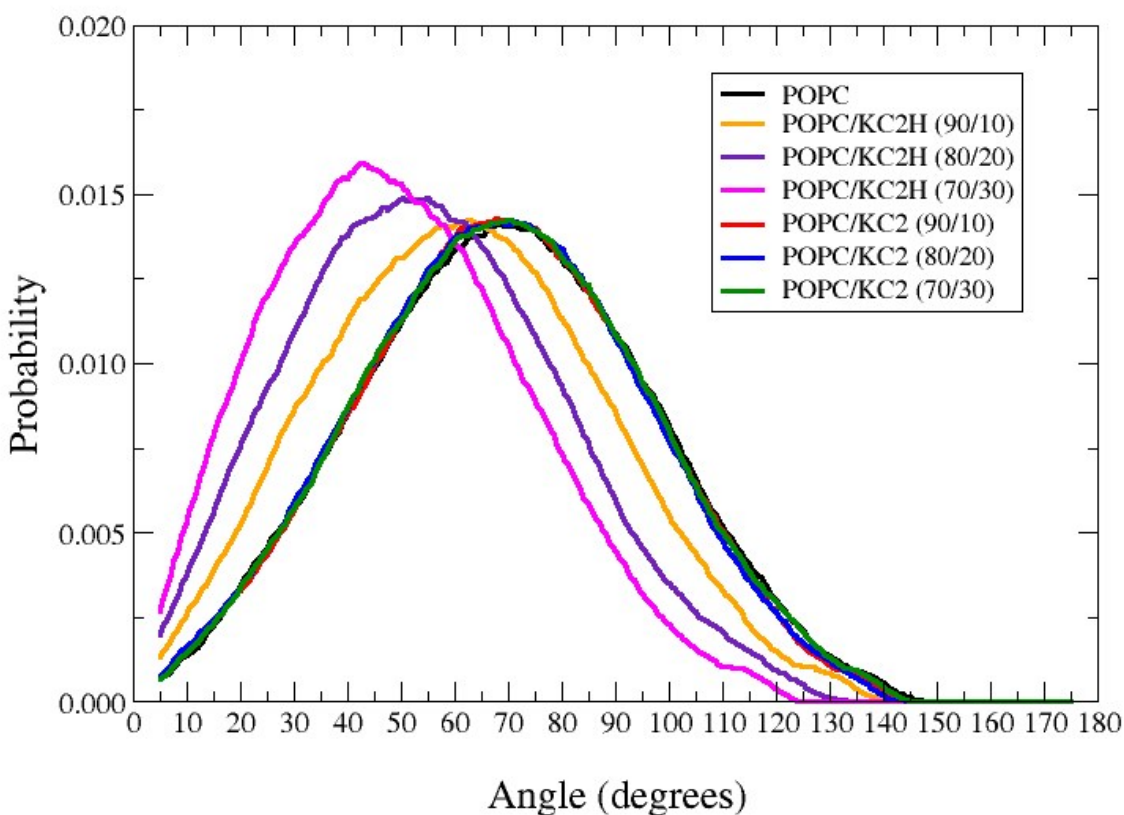


Figure S7. Effect of KC2 and KC2H on POPC P→N vector angle distribution. POPC headgroup angle distribution for each simulated system at $T = 313$ K are shown. The X axis shows the angle between the POPC P→N vector with the outward direction normal to the leaflet. Adding KC2H to the system reduces the POPC headgroup tilt angle at the acidic conditions but leaves it intact at the basic condition (systems with KC2).

Similar to the change in the ion distributions, the POPC headgroup will also interact with cationic lipids in the system. These electrostatic interactions will straighten the POPC headgroup and move the choline group to the aqueous phase [34, 44]. Consistent with what was observed in a study by Gurtovenko et al. [34] on zwitterionic-cationic lipid mixtures, including positively charged lipids in the PC bilayer shifts the PC headgroup tilt angle to the smaller angles, i.e. make it more perpendicular to the bilayer surface. The

observed changes in the POPC headgroup tilt angle in this study might partially explain why adding KC2H to the POPC dispersions results in smaller vesicles [2].

References:

- [1]. Semple, S.C., Akinc, A., Chen, J., Sandhu, A.P., Mui, B.L., Cho, C.K., Sah, D.W., Stebbing, D., Crosley, E.J., Yaworski, E. & Hafez, I. M. (2010). Rational design of cationic lipids for siRNA delivery. *Nature Biotechnology*, 28(2), 172-176.
- [2]. Kulkarni, J.A., Darjuan, M.M., Mercer, J.E., Chen, S., van der Meel, R., Thewalt, J.L., Tam, Y.Y.C. & Cullis, P. R. (2018). On the formation and morphology of lipid nanoparticles containing ionizable cationic lipids and siRNA. *ACS nano*, 12(5), 4787-4795.
- [3]. Hirota, S., de Ilarduya, C. T., Barron, L. G., & Szoka Jr, F. C. (1999). Simple mixing device to reproducibly prepare cationic lipid-DNA complexes (lipoplexes). *Biotechniques*, 27(2), 286-290.
- [4]. Jeffs, L. B., Palmer, L. R., Ambegia, E. G., Giesbrecht, C., Ewanick, S., & MacLachlan, I. (2005). A scalable, extrusion-free method for efficient liposomal encapsulation of plasmid DNA. *Pharmaceutical Research*, 22(3), 362-372.
- [5]. Kulkarni, J. A., Tam, Y. Y. C., Chen, S., Tam, Y. K., Zaifman, J., Cullis, P. R., & Biswas, S. (2017). Rapid synthesis of lipid nanoparticles containing hydrophobic inorganic nanoparticles. *Nanoscale*, 9(36), 13600-13609.
- [6]. Zhigaltsev, I. V., Belliveau, N., Hafez, I., Leung, A. K., Huft, J., Hansen, C., & Cullis, P. R. (2012). Bottom-up design and synthesis of limit size lipid nanoparticle systems with aqueous and triglyceride cores using millisecond microfluidic mixing. *Langmuir*, 28(7), 3633-3640.
- [7]. Zhigaltsev, I. V., Tam, Y. K., Leung, A. K., & Cullis, P. R. (2016). Production of limit size nanoliposomal systems with potential utility as ultra-small drug delivery agents. *Journal of Liposome Research*, 26(2), 96-102.

- [8]. Sternin, E., Bloom, M., & Mackay, A. L. (1983). De-Pake-ing of NMR spectra. *Journal of Magnetic Resonance*, 55(2), 274-282.
- [9]. Lafleur, M., Fine, B., Sternin, E., Cullis, P. R., & Bloom, M. (1989). Smoothed orientational order profile of lipid bilayers by ²H-nuclear magnetic resonance. *Biophysical Journal*, 56(5), 1037-1041.
- [10]. Schnablegger, H., & Singh, Y. (2013). The SAXS guide. *Anton Paar GmbH*.
- [11]. Hess, B., Kutzner, C., Van Der Spoel, D., & Lindahl, E. (2008). GROMACS 4: Algorithms for highly efficient, load-balanced, and scalable molecular simulation. *Journal of Chemical Theory and Computation*, 4(3), 435-447.
- [12]. Klauda, J.B., Venable, R.M., Freites, J.A., O'Connor, J.W., Tobias, D.J., Mondragon-Ramirez, C., Vorobyov, I., MacKerell Jr, A.D. & Pastor, R. W. (2010). Update of the CHARMM all-atom additive force field for lipids: Validation on six lipid types. *The Journal of Physical Chemistry B*, 114(23), 7830-7843.
- [13]. Durell, S. R., Brooks, B. R., & Ben-Naim, A. (1994). Solvent-induced forces between two hydrophilic groups. *The Journal of Physical Chemistry*, 98(8), 2198-2202.
- [14]. Jorgensen, W. L., Chandrasekhar, J., Madura, J. D., Impey, R. W., & Klein, M. L. (1983). Comparison of simple potential functions for simulating liquid water. *The Journal of Chemical Physics*, 79(2), 926-935.
- [15]. Parrinello, M., & Rahman, A. (1981). Polymorphic transitions in single crystals: A new molecular dynamics method. *Journal of Applied physics*, 52(12), 7182-7190.
- [16]. Nosé, S., & Klein, M. L. (1983). Constant pressure molecular dynamics for molecular systems. *Molecular Physics*, 50(5), 1055-1076.
- [17]. Nosé, S. (1984). A molecular dynamics method for simulations in the canonical ensemble. *Molecular physics*, 52(2), 255-268.
- [18]. Hoover, W. G. (1985). Canonical dynamics: Equilibrium phase-space distributions. *Physical Review A*, 31(3), 1695-1697.

- [19]. Darden, T., York, D., & Pedersen, L. (1993). Particle mesh Ewald: An N·log(N) method for Ewald sums in large systems. *The Journal of Chemical Physics*, 98(12), 10089-10092.
- [20]. Essmann, U., Perera, L., Berkowitz, M. L., Darden, T., Lee, H., & Pedersen, L. G. (1995). A smooth particle mesh Ewald method. *The Journal of Chemical Physics*, 103(19), 8577-8593.
- [21]. Hess, B., Bekker, H., Berendsen, H. J., & Fraaije, J. G. (1997). LINCS: A linear constraint solver for molecular simulations. *Journal of Computational Chemistry*, 18(12), 1463-1472.
- [22]. Lee, J., Cheng, X., Swails, J.M., Yeom, M.S., Eastman, P.K., Lemkul, J.A., Wei, S., Buckner, J., Jeong, J.C., Qi, Y. & Jo, S. (2015). CHARMM-GUI input generator for NAMD, GROMACS, AMBER, OpenMM, and CHARMM/OpenMM simulations using the CHARMM36 additive force field. *Journal of Chemical Theory and Computation*, 12(1), 405-413.
- [23]. Pluhackova, K., Kirsch, S. A., Han, J., Sun, L., Jiang, Z., Unruh, T., & Böckmann, R. A. (2016). A critical comparison of biomembrane force fields: Structure and dynamics of model DMPC, POPC, and POPE bilayers. *The Journal of Physical Chemistry B*, 120(16), 3888-3903.
- [24]. Humphrey, W., Dalke, A., & Schulten, K. (1996). VMD: Visual molecular dynamics. *Journal of Molecular Graphics*, 14(1), 33-38.
- [25]. Piggot, T. J., Allison, J. R., Sessions, R. B., & Essex, J. W. (2017). On the calculation of acyl chain order parameters from lipid simulations. *Journal of Chemical Theory and Computation*, 13(11), 5683-5696.
- [26]. Foloppe, N., & MacKerell, Jr, A. D. (2000). All-atom empirical force field for nucleic acids: I. Parameter optimization based on small molecule and condensed phase macromolecular target data. *Journal of Computational Chemistry*, 21(2), 86-104.
- [27]. Vanommeslaeghe, K., Hatcher, E., Acharya, C., Kundu, S., Zhong, S., Shim, J., Darian, E., Guvench, O., Lopes, P., Vorobyov, I. & Mackerell Jr, A. D. (2010). CHARMM general force field: A force field for drug-like molecules compatible with the CHARMM all-atom additive biological force fields. *Journal of Computational Chemistry*, 31(4), 671-690.

- [28]. Jo, S., Kim, T., Iyer, V. G., & Im, W. (2008). CHARMM-GUI: A web-based graphical user interface for CHARMM. *Journal of Computational Chemistry*, 29(11), 1859-1865.
- [29]. Huang, L., & Roux, B. (2013). Automated force field parameterization for nonpolarizable and polarizable atomic models based on ab initio target data. *Journal of Chemical Theory and Computation*, 9(8), 3543-3556.
- [30]. Vanommeslaeghe, K., & MacKerell Jr, A. D. (2012). Automation of the CHARMM General Force Field (CGenFF) I: Bond perception and atom typing. *Journal of Chemical Information and Modeling*, 52(12), 3144-3154.
- [31]. Vanommeslaeghe, K., Raman, E. P., & MacKerell Jr, A. D. (2012). Automation of the CHARMM General Force Field (CGenFF) II: Assignment of bonded parameters and partial atomic charges. *Journal of Chemical Information and Modeling*, 52(12), 3155-3168.
- [32]. Ramezanpour, M. (2019). *Computer simulation of biomolecular systems of interest in bionanotechnology* (Doctoral Dissertation, Science: Department of Biological Sciences).
- [33]. Petelska, A. D., & Figaszewski, Z. A. (2000). Effect of pH on the interfacial tension of lipid bilayer membrane. *Biophysical Journal*, 78(2), 812-817.
- [34]. Gurtovenko, A. A., Patra, M., Karttunen, M., & Vattulainen, I. (2004). Cationic DMPC/DMTAP lipid bilayers: Molecular dynamics study. *Biophysical Journal*, 86(6), 3461-3472.
- [35]. Pandit, S. A., Bostick, D., & Berkowitz, M. L. (2003). Molecular dynamics simulation of a dipalmitoylphosphatidylcholine bilayer with NaCl. *Biophysical Journal*, 84(6), 3743-3750.
- [36]. Pandit, S. A., Bostick, D., & Berkowitz, M. L. (2003). Mixed bilayer containing dipalmitoylphosphatidylcholine and dipalmitoylphosphatidylserine: Lipid complexation, ion binding, and electrostatics. *Biophysical Journal*, 85(5), 3120-3131.
- [37]. Marrink, S. J., Sok, R. M., & Berendsen, H. J. C. (1996). Free volume properties of a simulated lipid membrane. *The Journal of Chemical Physics*, 104(22), 9090-9099.

- [38]. Kupiainen, M., Falck, E., Ollila, S., Niemelä, P., Gurtovenko, A.A., Hyvönen, M.T., Patra, M., Karttunen, M. & Vattulainen, I. (2005). Free volume properties of sphingomyelin, DMPC, DPPC, and PLPC bilayers. *Journal of Computational and Theoretical Nanoscience*, 2(3), 401-413.
- [39]. Navas, B.P., Lohner, K., Deutsch, G., Sevcsik, E., Riske, K.A., Dimova, R., Garidel, P. & Pabst, G. (2005). Composition dependence of vesicle morphology and mixing properties in a bacterial model membrane system. *Biochimica et Biophysica Acta (BBA)-Biomembranes*, 1716(1), 40-48.
- [40]. Gurtovenko, A. A., Miettinen, M., Karttunen, M., & Vattulainen, I. (2005). Effect of monovalent salt on cationic lipid membranes as revealed by molecular dynamics simulations. *The Journal of Physical Chemistry B*, 109(44), 21126-21134.
- [41]. Böckmann, R. A., Hac, A., Heimburg, T., & Grubmüller, H. (2003). Effect of sodium chloride on a lipid bilayer. *Biophysical Journal*, 85(3), 1647-1655.
- [42]. Doux, J. P., Hall, B. A., & Killian, J. A. (2012). How lipid headgroups sense the membrane environment: An application of ^{14}N NMR. *Biophysical Journal*, 103(6), 1245-1253.
- [43]. Semchyschyn, D. J., & Macdonald, P. M. (2004). Conformational response of the phosphatidylcholine headgroup to bilayer surface charge: Torsion angle constraints from dipolar and quadrupolar couplings in bicelles. *Magnetic Resonance in Chemistry*, 42(2), 89-104.
- [44]. Bechinger, B., & Seelig, J. (1991). Interaction of electric dipoles with phospholipid head groups. A deuterium and phosphorus-31 NMR study of phloretin and phloretin analogs in phosphatidylcholine membranes. *Biochemistry*, 30(16), 3923-3929.